Chemical Science

EDGE ARTICLE

View Article Online
View Journal | View Issue

Cite this: *Chem. Sci.*, 2019, **10**, 10870

All publication charges for this article have been paid for by the Royal Society of Chemistry

Received 25th September 2019
Accepted 15th October 2019

DOI: 10.1039/c9sc04832d

rsc.li/chemical-science

$LiMg(IO_3)_3$: an excellent SHG material designed by single-site aliovalent substitution†

Jin Chen,[ab] Chun-Li Hu,*[a] Fei-Fei Mao,[c] Xiao-Han Zhang,[a] Bing-Ping Yang[a] and Jiang-Gao Mao*[a]

An excellent second harmonic generation (SHG) material, $LiMg(IO_3)_3$ (LMIO), has been elaborately designed from $Li_2M^{IV}(IO_3)_6$ (M^{IV} = Ti, Sn, and Ge) by aliovalent substitution of the central M^{IV} cation followed by Wyckoff position exchange. The new structure sustains the ideal-alignment of $(IO_3)^-$ groups. Importantly, LMIO exhibits an extremely strong SHG effect of roughly 24 × KH_2PO_4 (KDP) under 1064 nm laser radiation or 1.5 × $AgGaS_2$ (AGS) under 2.05 μm laser radiation, which is larger than that of α-$LiIO_3$ (18 × KDP). The replacement of M^{IV} with Mg^{2+} without d–d electronic transitions induces an obviously larger band gap (4.34 eV) with a short absorption edge (285 nm). This study shows that single-site aliovalent substitution provides a new synthetic route for designing SHG materials.

Introduction

Noncentrosymmetric (NCS) or polar crystals have attracted scientific endeavors since they are potential candidates as SHG materials.[1,2] Metal iodates with polar units, $(IO_3)^-$ or $(IO_4)^{3-}$, are a class of important compounds which can exhibit excellent SHG performance.[3] Numerous synthetic efforts have been made and afforded a number of iodates with outstanding SHG properties,[3–8] such as $BiO(IO_3)$ (12.5 × KDP)[7a] and GdI_5O_{14} (15 × KDP).[8d] However, generally, the larger SHG effects of iodates are usually accompanied by smaller band gaps. Recently, aliovalent substitution has become an effective approach for exploring novel SHG crystals.[9,10] Aliovalent substitution of $BiO(IO_3)$ gave $BiFSeO_3$, which has the highest SHG effect among selenites reported.[9a] The novel route of aliovalent substitution involving three atom sites has expended d^0-TM cations to post main group cations, such as from V^{5+} to Ga^{3+}.[10] In this way, isostructural compounds sustained both large polarizability and a wide band gap.[10] For example, α- and β-$Ba_2[GaF_4(IO_3)_2(IO_3)]$ (6 × KDP; 4.61 and 4.31 eV)[10a] have clearly larger band gaps and slightly weaker SHG signals than α- and β-$Ba_2[VO_2F_4(IO_3)_2(IO_3)]$ (9 × KDP; 2.59 and 2.55 eV).[9d]

Recently, a serial of isostructural SHG iodates, namely $Li_2M^{IV}(IO_3)_6$ (M^{IV} = Ti, Sn, and Ge), were reported, whose structures feature well-arranged $(IO_3)^-$ units. The regulation of Ti^{4+}, Sn^{4+} and Ge^{4+} cations induces SHG effects shifting from 17×, 15×, to 32 × KDP and band gaps changing from 3.0, 3.9 to 3.89 eV for Ti, Sn and Ge compounds, respectively.[11] Interestingly, in these structures, both Li^+ and M^{4+} cations are octahedrally coordinated but they occupy different Wyckoff positions. The Li^+ cation site on 2b and the LiO_6 octahedra are bridged by iodate groups into a 3D $[Li(IO_3)_6]^{5-}$ framework. M^{4+} cations located at 2a are only 50% occupied and 0D $[M^{IV}(IO_3)_6]^{2-}$ polyanions were formed. The full occupation of M^{IV} would be not consistent with the colorless and insulating crystals, which had been discussed in detail by P. Shiv Halasyamani.[11b] We consider that aliovalent substitution of the M^{4+} cation with two divalent metal ions may result in $LiM^{II}(IO_3)_3$ with a completely ordered structure, and this expands the family of this class of metal iodates with excellent SHG effects. Additionally, the use of alkaline-earth cations can avoid the unfavorable d–d electronic transitions for the transition metal ions and favors the blue-shift of the absorption edge. By using such a single-site aliovalent substitution method, $LiMg(IO_3)_3$ (LMIO) was designed from $Li_2M^{IV}(IO_3)_6$ *via* replacing the defect-containing M^{4+} cation with an ordered Mg^{2+} cation followed by Wyckoff position exchange. In LMIO, a 3D $[Mg(IO_3)_6]^{4-}$ anionic framework is formed instead of 0D $[M^{IV}(IO_3)_6]^{2-}$ anions. LMIO displays an extremely large SHG response (24 × KDP under 1064 nm laser radiation or 1.5 × AGS under 2.05 μm laser radiation), large band gap (4.34 eV), high LDT (46 × AGS) and good thermal stability (>500 °C).

Results and discussion

Polar LMIO was prepared by hydrothermal reactions of LiCl, $MgCl_2$, I_2O_5 and 3% HCl solution at 230 °C for 3 days. Its purity

[a]*State Key Laboratory of Structural Chemistry, Fujian Institute of Research on the Structure of Matter, Chinese Academy of Sciences, Fuzhou 350002, P. R. China. E-mail: mjg@fjirsm.ac.cn; clhu@fjirsm.ac.cn*

[b]*University of Chinese Academy of Sciences, Beijing 100039, P. R. China*

[c]*Nanjing Agricultural University, Nanjing 210095, P. R. China*

† Electronic supplementary information (ESI) available. CCDC 1951165. For ESI and crystallographic data in CIF or other electronic format see DOI: 10.1039/c9sc04832d

was checked by PXRD study and EDS elemental analyses (Fig. S1 and S2†).

LMIO crystallizes in the NCS and polar space group $P6_3$ (no. 173). The asymmetric unit of LMIO contains one Li, one Mg, one I, and three O atoms. Both Li and Mg atoms occupy sites with 3-fold axis symmetry whereas the remaining atoms are located at the normal sites. Both Li^+ and Mg^{2+} cations connect with six O atoms to form LiO_6 and MgO_6 octahedra, and each octahedron links with six $(IO_3)^-$ groups which are ideally aligned along the *c* direction, leading to very large polarizability. The lengths of the Li–O bond (2.075(6) and 2.088(5) Å) and Mg–O bond (2.076(2) and 2.111(2) Å) are pretty close indicating that the distortions of LiO_6 and MgO_6 are very small. The I^{5+} atom is three coordinated in a triangular-pyramidal geometry with I–O bond lengths of 1.7966(19), 1.809(2) and 1.815(2) Å. BVS calculations exhibit the values of 1.14 (Li), 2.03 (Mg) and 5.06 (I), verifying that these cations are in oxidation states of +1, +2 and +5, respectively.

Neighboring LiO_6 octahedra are inter-linked into a 1D chain along the *c*-axis *via* face-sharing (Fig. 1a) whereas neighboring MgO_6 octahedra are bridged by iodate groups into a 3D $[Mg(IO_3)_6]^{4-}$ anionic framework with 1D tunnels of Mg_6I_6 12-membered rings (MRs) (Fig. 1b). The overall structure of LMIO can be viewed as the 1D chains of face-sharing LiO_6 octahedra inserted into the 1D tunnels of the 3D $[Mg(IO_3)_6]^{4-}$ anionic framework (Fig. 1c). Because that a process of Wyckoff position exchange occurred as the structural evolution from $Li_2M^{IV}(IO_3)_6$ to LMIO and different occupancy of the cation at the 2a position (fully occupied Li^+ in LMIO but 50% occupied M^{4+} in $Li_2M^{IV}(IO_3)_6$), it is interesting to note that there is in the structures of $Li_2M^{IV}(IO_3)_6$ (M = Ti, Sn, Ge), neighboring LiO_6 octahedra or $[M^{IV}(IO_3)_6]^{2-}$ anions are not interconnected, that is they are isolated.[11]

The ionic radii of the six-coordinated Li^+, Mg^{2+}, Ti^{4+}, Sn^{4+}, and Ge^{4+} are 0.076, 0.072, 0.0605, 0.069, and 0.053 nm, respectively.[12] Obviously, the ionic radius of Mg^{2+} is much closer to that of Li^+ than that of M^{4+}. Thus, Wyckoff position exchange occurred during the aliovalent substitution of M^{4+} with Mg^{2+} cations. In addition, our calculations of total energy show that LMIO (−12 816.63 eV) is more energy-favorable than the one adopting the $Li_2M^{IV}(IO_3)_6$ (M = Ti, Sn, Ge) structural type (−12814.03 eV). Attempts to replace Li^+ in LMIO with Na^+ to get an isostructural sodium phase were not successful, probably owing to the much larger size of Na^+ (0.102 nm). We consider that a disordered M^{3+} cation, such as Al^{3+} and Ga^{3+} with 67% occupancy, may replace the M^{4+} cation in $Li_2M^{IV}(IO_3)_6$ (M = Ti, Sn, Ge).

The calculations of bond strain index (BSI) and global instability index (GII) values gave small values of 0.030 (BSI) and 0.079 (GII) for LMIO, which indicated that the structure of LMIO is unstrained and stable.[11b,13] The corresponding BSI and GII values of $Li_2M^{IV}(IO_3)_6$ (M = Ti, Sn, Ge) are much larger than those of LMIO (Table S3†), which are consistent with the disorder in $Li_2M^{IV}(IO_3)_6$ (M = Ti, Sn, Ge).

Thermogravimetric analysis (TGA) reveals the high thermal stability (>500 °C) of LMIO (Fig. 2). It shows two steps of weight loss in 500–650 °C (sharp) and 750–910 °C (smooth), and both are related to the release of I_2 and O_2. The DSC curves exhibit

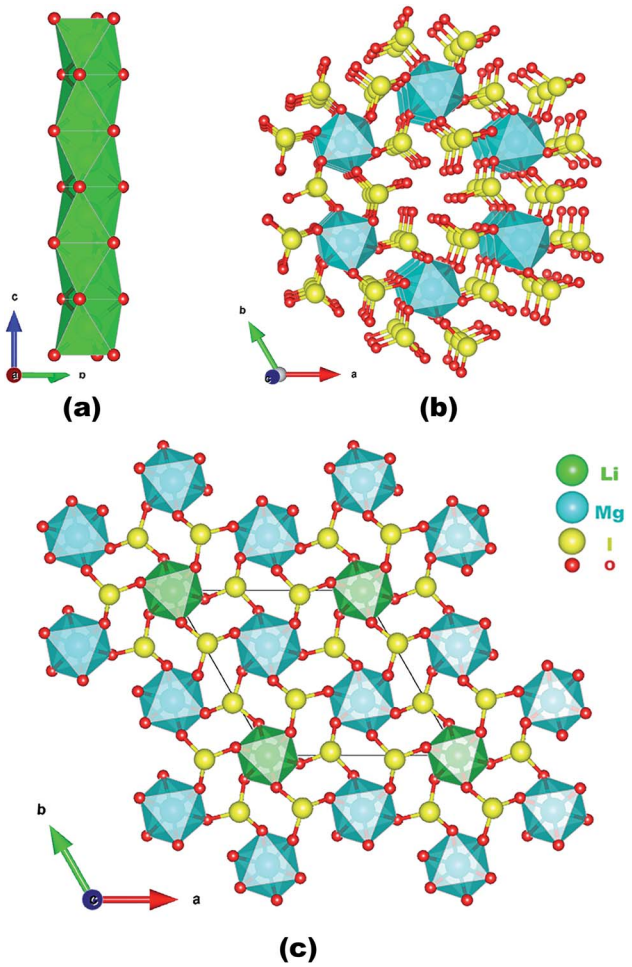

Fig. 1 A 1D chain of face-sharing LiO_6 octahedra along the *c*-axis (a); the 3D $[Mg(IO_3)_6]^{4-}$ anionic framework along the *c*-axis (b); and the view of the structure of LMIO along the *c*-axis (c).

three endothermic peaks at 610, 647 and 903 °C and one exothermic peak at 626 °C. Compared to $Li_2M^{IV}(IO_3)_6$ (M = Ti, Sn, Ge) (~400 °C), LMIO has higher thermal stability.[11]

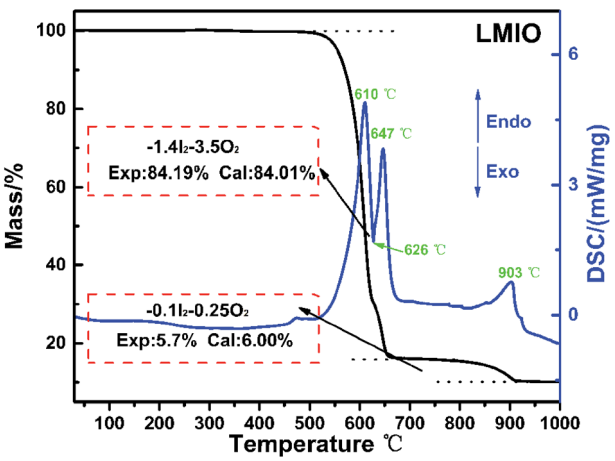

Fig. 2 TG and DSC analyses of LMIO.

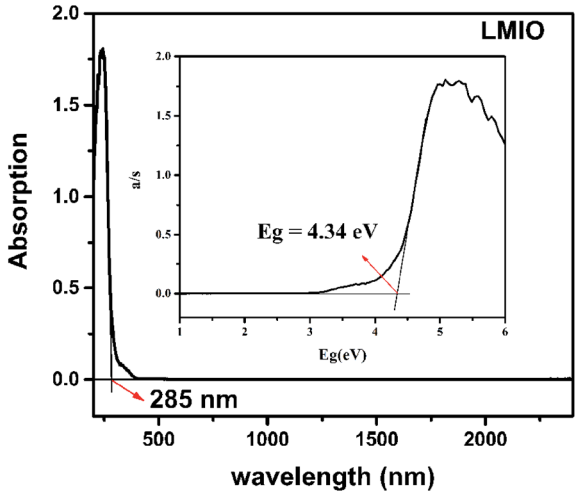

Fig. 3 UV-Vis-IR analysis of LMIO.

The IR spectrum shows that LMIO is transparent in the wavelength region of 2.5–11.2 μm (4000–890 cm^{-1}) (Fig. S3†). The UV-Vis-IR study revealed the absorption edge of 285 nm for LMIO (Fig. 3). Hence, the transparent range (0.28–11.2 μm) of LMIO covers the UV, Visible and mid-IR regions. The band gap of LMIO (4.34 eV) is significantly wider than those of Li_2-$M^{IV}(IO_3)_6$ (M = Ti, Sn, Ge) (3.0, 3.9 and 3.86 eV for Ti, Sn and Ge compounds, respectively).[11]

Powder SHG experiments indicate that LMIO is a phase-matchable SHG material with remarkable SHG signals of 24 × KDP under 1064 nm laser radiation or 1.5 × AGS under 2.05 μm laser radiation (Fig. 4). Compared with commercial α-$LiIO_3$ (18 × KDP), LMIO possesses an obviously enhanced SHG signal. The SHG response of LMIO is also much larger than those of $Li_2Ti(IO_3)_6$ (17 × KDP) and $Li_2Sn(IO_3)_6$ (15 × KDP) but is slightly smaller than that of $Li_2Ge(IO_3)_6$ (32 × KDP). Eliminating the influence induced by the disorder effect, we adopt the Gaussian09 program to calculate the first-order

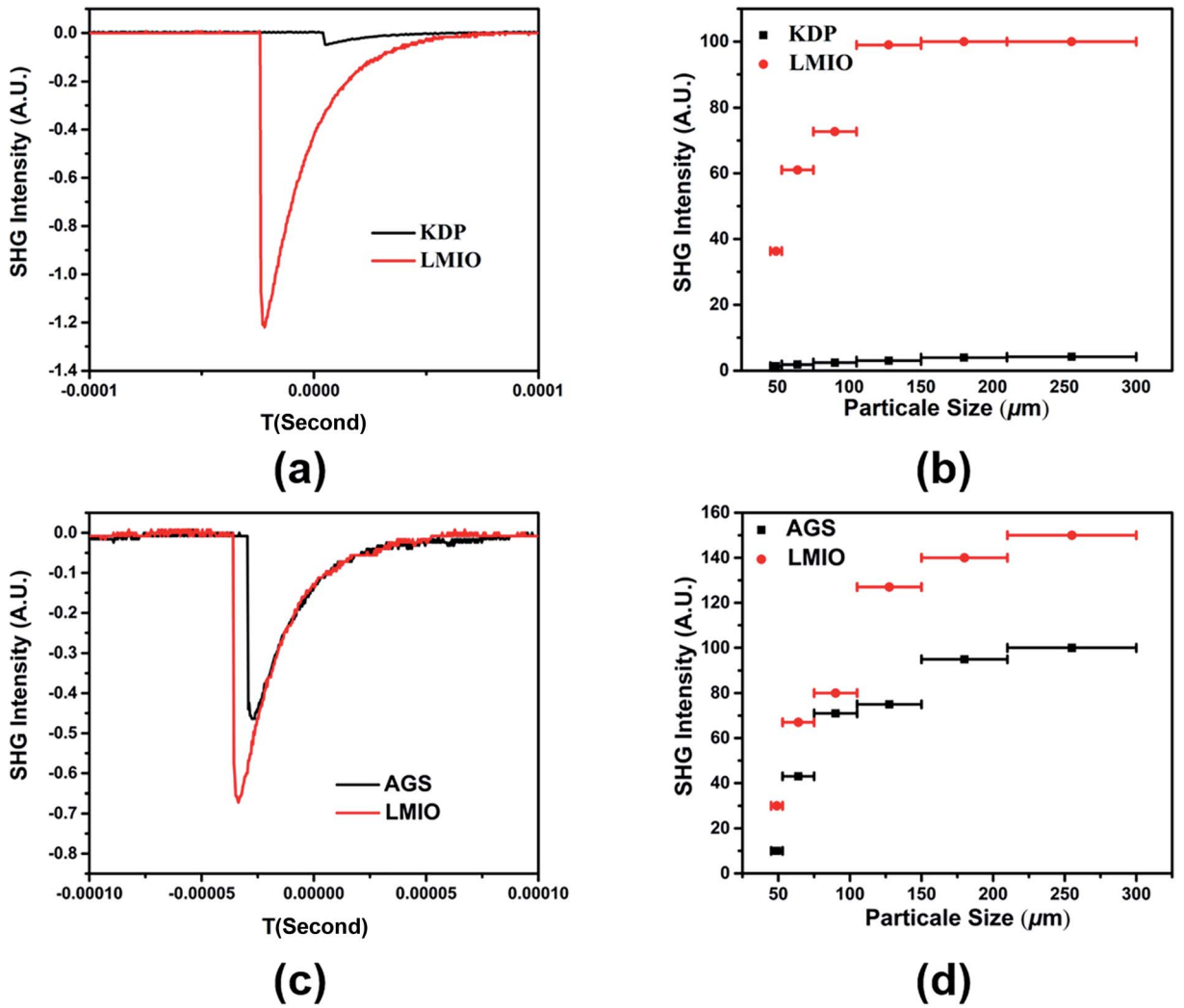

Fig. 4 Oscilloscope traces of the SHG signal (150–210 mm) of LMIO at (a) 1064 nm and (c) 2.05 μm. Plots of measured SHG intensity *vs.* particle size of LMIO under laser radiation at (b) 1064 nm and (d) 2.05 μm. KDP and AGS samples serve as the references for 1064 and 2.05 μm laser radiation, respectively.

hyperpolarizabilities of $[Mg(IO_3)_6]^{4-}$ and $[M^{IV}(IO_3)_6]^{2-}$ anions (M = Ti, Sn and Ge), which are obtained to be 3047, 2982, 2602 and 1707 a.u. for Ge, Mg, Sn, and Ti, respectively, and such a trend is roughly consistent with results from the SHG measurements ($Li_2Ge(IO_3)_6$ > LMIO > $Li_2Sn(IO_3)_6 \approx Li_2Ti(IO_3)_6$). Notably, LMIO is the only NLO material featuring excellent optical nonlinearity (>20 × KDP) and a near-UV absorption edge (<300 nm).

LDT experiments revealed a large value of 101.86 MW cm^{-2} for LMIO, which is about 46 times that of AGS (2.22 MW cm^{-2}). This value is comparable to those of $Li_2M^{IV}(IO_3)_6$ (M = Ti, Sn, Ge) (49×, 41×, and 42 × AGS for Ti, Sn and Ge compounds, respectively) and α-$LiIO_3$ (54 × AGS).[11d]

Theoretical calculations based on DFT methods were applied for understanding the source of the outstanding SHG effect. Band structure calculations revealed that LMIO is an indirect band gap compound with a gap of 3.35 eV (Fig. S4†), which is much smaller than the measured value (4.34 eV). Hence scissor of 0.99 eV was applied during the subsequent optical property analyses.

The partial density of states (PDOS) was studied for the energy band assignment and bond interaction (Fig. 5). In the whole energy region, full overlapping of the electronic states between I atoms and O atoms is observed, indicating strong interactions in I–O bonds. The band gap of LMIO is determined by IO_3 units because the nonbonding orbitals from I and O

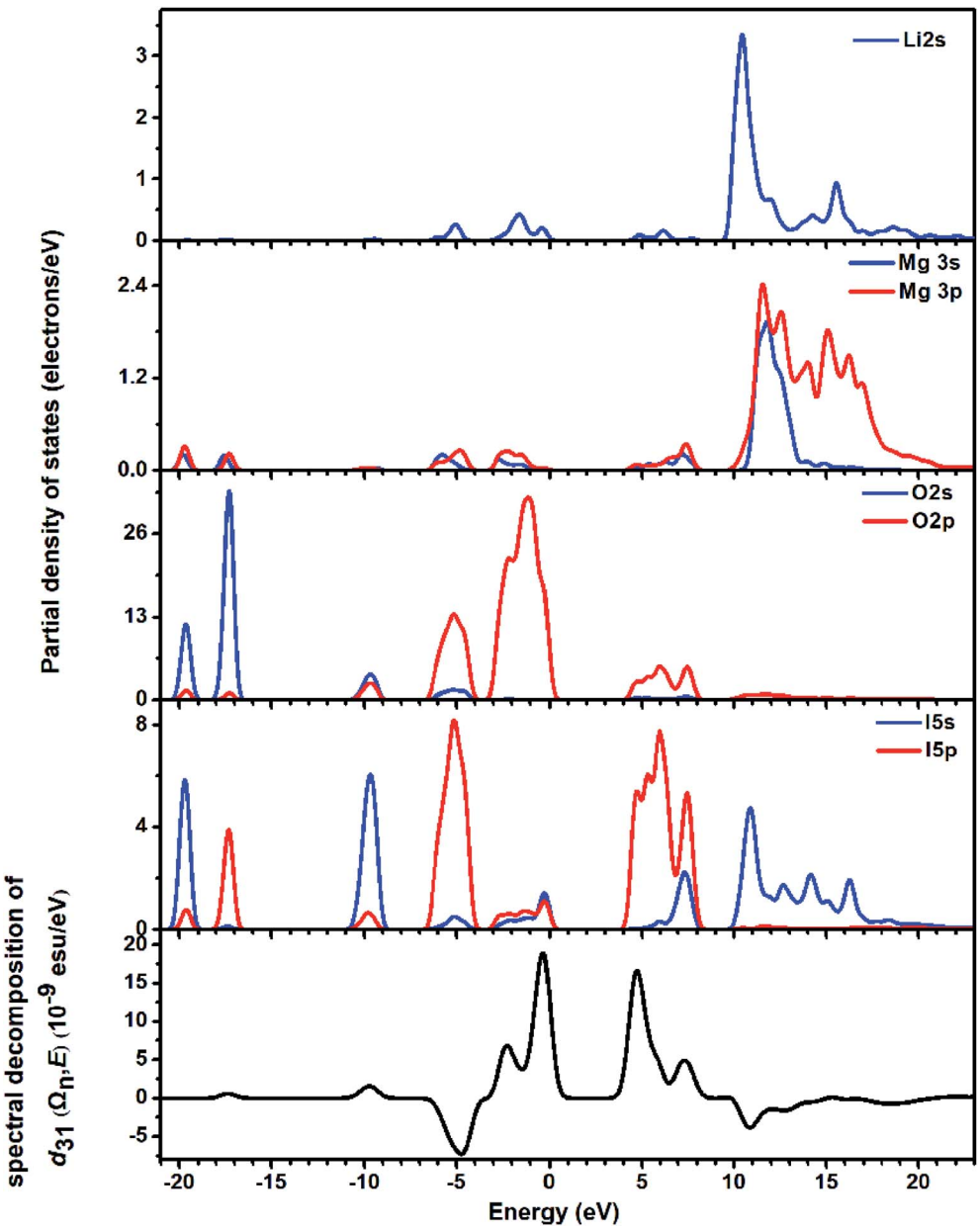

Fig. 5 The partial density of states (the upper four panels) and the spectral decomposition of d_{31} (the bottommost panel) for LMIO.

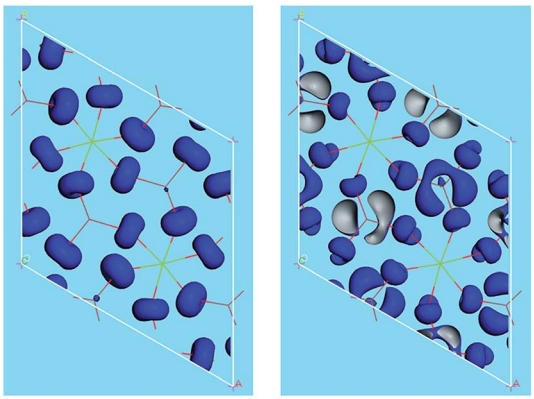

Fig. 6 The SHG density of d_{31} in the VB (a) and CB for LMIO (b).

atoms dominate the highest VB; meanwhile the empty orbitals from I and O atoms define the lowest CB.

Calculations of the SHG coefficient of LMIO revealed the largest SHG tensor d_{31} of 2.02 × 10^{-8} esu at 1064 nm. This result is consistent with our experimental value (24 × KDP). In addition, the refractive index curves of LMIO were recorded. It shows large anisotropy with large birefringence at 1064 nm (0.22), ensuring phase-matching abilities (Fig. S5†).

The SHG origin of LMIO has been further explored from spectral decomposition and SHG density. The spectral decomposition plot of d_{31} (the bottom panel in Fig. 5) indicates that the main SHG-contributed regions are located at the upper part of the VB and the lower part of the CB, corresponding to O-2p nonbonding states and unoccupied I-5p and O-2p states, respectively. There are small negative contributions from the VB regions of −6.3 to −3.6 eV and the CB region of 10–15 eV. Intuitively, for the SHG density (Fig. 6), the major SHG-contributors are the O-2p nonbonding orbitals in the VB and the unoccupied O-2p and I-5p orbitals in the CB. Accordingly, the IO_3 building units are the leading source of the large SHG coefficient. Numerically, the SHG-contributed percentages of Li^+, MgO_6 and IO_3 groups are 0.43%, 8.94% and 90.6%, respectively. Hence, it is concluded that the very strong SHG response of LMIO originates predominantly from the ideal-alignment of $(IO_3)^-$ groups.

Conclusions

In conclusion, *via* the aliovalent substitution of disordered M^{IV} (50% occupancy) with fully ordered Mg^{2+} and the exchange of Wyckoff positions, a promising SHG material, $LiMg(IO_3)_3$ (LMIO), has been obtained. It displays a strong SHG effect (24 × KDP) with a phase matching ability and large band gap (4.34 eV). LMIO also has superior thermal stability (>500 °C) and LDT properties (46 × AGS). This novel approach of replacement of M^{IV} by M^{II} atoms further expands the family of iodate-based SHG materials. Our future research efforts will be devoted to aliovalent substitution of M^{IV} with defect containing M^{III} (66.7% occupancy) cations.

Conflicts of interest

The authors declare no competing financial interest.

Acknowledgements

Our work has been supported by the National Natural Science Foundation of China (No. 21231006, 91622112, 21875248 and 21773244), the Strategic Priority Research Program of the Chinese Academy of Sciences (XDB20000000), and the 100 Talents Project of Fujian Province. We thank Bingxuan Li at FJIRSM for their help with the laser-induced damage threshold (LDT) tests.

Notes and references

1 (*a*) S. P. Guo, X. Cheng, Z. D. Sun, Y. Chi, B. W. Liu, X. M. Jiang, S. F. Li, H. G. Xue, S. Deng, V. Duppel, J. Khler and G. C. Guo, *Angew. Chem., Int. Ed.*, 2019, **58**, 8087–8091; *Angew. Chem.*, 2019, **131**, 8171–8175; (*b*) H. M. Zhou, L. Xiong, L. Chen and L. M. Wu, *Angew. Chem., Int. Ed.*, 2019, **58**, 9979–9983; *Angew. Chem.*, 2019, **131**, 10084–10088; (*c*) B. Zhang, E. Tikhonov, C. Xie, Z. Yang and S. Pan, *Angew. Chem., Int. Ed.*, 2019, **58**, 11726–11730; *Angew. Chem.*, 2019, **131**, 11852–11856; (*d*) L. Kang, X. Zhang, F. Liang, Z. Lin and B. Huang, *Angew. Chem., Int. Ed.*, 2019, **58**, 10250–10254; *Angew. Chem.*, 2019, **131**, 10356–10360; (*e*) B. L. Wu, C. L. Hu, F. F. Mao, R. L. Tang and J. G. Mao, *J. Am. Chem. Soc.*, 2019, **141**, 10188–10192; (*f*) J. Mark, J. Wang, K. Wu, J. G. Lo, S. Lee and K. Kovnir, *J. Am. Chem. Soc.*, 2019, **141**, 11976–11983.

2 (*a*) K. M. Ok, *Acc. Chem. Res.*, 2016, **49**, 2774–2785; (*b*) Z. Xia and K. R. Poeppelmeier, *Acc. Chem. Res.*, 2017, **50**, 1222–1230; (*c*) M. Mutailipu, M. Zhang, Z. Yang and S. Pan, *Acc. Chem. Res.*, 2019, **52**, 791–801; (*d*) S. P. Guo, Y. Chi and G. C. Guo, *Coord. Chem. Rev.*, 2017, **355**, 44–57.

3 (*a*) M. S. Wickleder, *Chem. Rev.*, 2002, **102**, 2011–2088; (*b*) C. L. Hu and J. G. Mao, *Coord. Chem. Rev.*, 2015, **288**, 1–17; (*c*) C. F. Sun, B. P. Yang and J. G. Mao, *Sci. China: Chem.*, 2011, **54**, 911–922.

4 (*a*) R. E. Sykora, K. M. Ok, P. S. Halasyamani and T. E. Albrecht-Schmitt, *J. Am. Chem. Soc.*, 2002, **124**, 1951–1957; (*b*) Y. H. Li, G. P. Han, H. W. Yu, H. Li, Z. H. Yang and S. L. Pan, *Chem. Mater.*, 2019, **31**, 2992–3000.

5 (*a*) R. E. Sykora, K. M. Ok, P. S. Halasyamani, D. M. Wells and T. E. Albrecht-Schmitt, *Chem. Mater.*, 2002, **14**, 2741–2749; (*b*) B. P. Yang, C. L. Hu, X. Xu, C. F. Sun, J. H. Zhang and J. G. Mao, *Chem. Mater.*, 2010, **22**, 1545–1550; (*c*) C. F. Sun, C. L. Hu, X. Xu, B. P. Yang and J. G. Mao, *J. Am. Chem. Soc.*, 2011, **133**, 5561–5572; (*d*) H. W. Yu, M. L. Nisbet and K. R. Poeppelmeier, *J. Am. Chem. Soc.*, 2018, **140**, 8868–8876.

6 (*a*) C. F. Sun, C. L. Hu, X. Xu, J. B. Ling, T. Hu, F. Kong, X. F. Long and J. G. Mao, *J. Am. Chem. Soc.*, 2009, **131**, 9486–9487; (*b*) F. F. Mao, C. L. Hu, J. Chen, R. L. Tang, B. L. Wu and J. G. Mao, *Chem. Commun.*, 2019, **55**, 6906–6909; (*c*) H. X. Tang, Y. X. Zhang, C. Zhou, R. B. Fu, H. Lin,

Z. J. Ma and X. T. Wu, *Angew. Chem., Int. Ed.*, 2019, **58**, 3824–3828; *Angew. Chem.*, 2019, **131**, 3864–3868.

7 (*a*) S. D. Nguyen, J. Yeon, S. H. Kim and P. S. Halasyamani, *J. Am. Chem. Soc.*, 2011, **133**, 12422–12425; (*b*) F. F. Mao, C. L. Hu, X. Xu, D. Yan, B. P. Yang and J. G. Mao, *Angew. Chem., Int. Ed.*, 2017, **129**, 2183–2187; *Angew. Chem.*, 2017, **129**, 2183–2187.

8 (*a*) K. M. Ok and P. S. Halasyamani, *Angew. Chem., Int. Ed.*, 2004, **43**, 5489–5491; *Angew. Chem.*, 2004, **116**, 5605–5607; (*b*) X. Xu, C. L. Hu, B. X. Li, B. P. Yang and J. G. Mao, *Chem. Mater.*, 2014, **26**, 3219–3230; (*c*) F. F. Mao, C. L. Hu, J. Chen, B. L. Wu and J. G. Mao, *Inorg. Chem.*, 2019, **58**, 3982–3989; (*d*) J. Chen, C. L. Hu, F. F. Mao, B. P. Yang, X. H. Zhang and J. G. Mao, *Angew. Chem., Int. Ed.*, 2019, **58**, 11666–11669; *Angew. Chem.*, 2019, **131**, 11792–11795.

9 (*a*) M. L. Liang, C. L. Hu, F. Kong and J. G. Mao, *J. Am. Chem. Soc.*, 2016, **128**, 9433–9436; (*b*) X. L. Cao, C. L. Hu, F. Kong and J. G. Mao, *Inorg. Chem.*, 2015, **54**, 3875–3882; (*c*) X. L. Cao, C. L. Hu, X. Xu, F. Kong and J. G. Mao, *Chem. Commun.*, 2013, **49**, 9965–9967; (*d*) X. H. Dong, L. Huang, C. F. Hu, H. M. Zeng, Z. Lin, X. Wang, G. H. Zou and K. M. OK, *Angew. Chem., Int. Ed.*, 2019, **58**, 6528–6534; *Angew. Chem.*, 2019, **131**, 6598–6604; (*e*) F. Yang, L. Huang, X. Zhao, L. Huang, D. Gao, J. Bi, X. Wang and G. Zou, *J. Mater. Chem. C*, 2019, **7**, 8131–8138.

10 (*a*) J. Chen, C. L. Hu, F. F. Mao, J. H. Feng and J. G. Mao, *Angew. Chem., Int. Ed.*, 2019, **58**, 2098–2102; *Angew. Chem.*, 2019, **131**, 2120–2124; (*b*) F. You, F. Liang, Q. Huang, Z. Hu, Y. Wu and Z. Lin, *J. Am. Chem. Soc.*, 2019, **141**, 748–752.

11 (*a*) H. Y. Chang, S. H. Kim, P. S. Halasyamani and K. M. Ok, *J. Am. Chem. Soc.*, 2009, **131**, 2426–2427; (*b*) H. Y. Chang, S. H. Kim, K. M. Ok and P. S. Halasyamani, *J. Am. Chem. Soc.*, 2009, **131**, 6865–6873; (*c*) H. Y. Kim, T. T. Tran, P. S. Halasyamani and K. M. Ok, *Inorg. Chem. Front.*, 2015, **2**, 361–368; (*d*) B. P. Yang, C. L. Hu, X. Xu and J. G. Mao, *Inorg. Chem.*, 2016, **55**, 2481–2487; (*e*) F. F. Mao, C. L. Hu, J. Chen and J. G. Mao, *Chem. Mater.*, 2018, **30**, 2443–2452; (*f*) H. M. Liu, X. X. Jiang, X. X. Wang, L. Yang, Z. S. Lin, Z. G. Hu, X. G. Meng, X. G. Chen and J. G. Qin, *J. Mater. Chem. C*, 2018, **6**, 4698–4705.

12 R. D. Shannon, *Acta Crystallogr., Sect. A: Cryst. Phys., Diffr., Theor. Gen. Crystallogr.*, 1976, **32**, 751–767.

13 (*a*) C. Preiser, J. Losel, I. D. Brown, M. Kunz and A. Skowron, *Acta Crystallogr., Sect. B: Struct. Sci.*, 1999, **B55**, 698–711; (*b*) A. Salinas-Sanchez, J. L. Garcia-Munoz, J. Rodriguez-Carvajal, R. SaezPuche and J. L. Martinez, *J. Solid State Chem.*, 1992, **100**, 201–211; (*c*) I. D. Brown, *The Chemical Bond in Inorganic Chemistry: The Bond Valence Model*, Oxford University Press, Oxford, U.K., 1st edn, 2002.